PROCEEDINGS OF SCIENCE

Modeling the gamma-ray emission from the Sun

Eleonora Puzzoni,[a,*] **Federico Fraschetti,**[a,b] **Jozsef Kota**[a] **and Joe Giacalone**[a]

[a] *University of Arizona, Lunar and Planetary Laboratory, 1629 E University Blvd, Tucson, AZ, USA*

[b] *Center for Astrophysics, Harvard & Smithsonian, 60 Garden Street, Cambridge, MA, USA*

E-mail: epuzzoni@arizona.edu, ffrasche@arizona.edu, jkota@arizona.edu, giacalon@arizona.edu

Despite its very close proximity to Earth and considerable previous study, there remain many unsolved puzzles about the Sun. One such example of significant recent interest relates to the GeV-TeV gamma-ray emission from the solar disk. Indeed, the only existing theoretical model can not fully explain the observed spectrum by Fermi Gamma-ray Space Telescope, which is significantly brighter and harder than predicted. Moreover, the theory fails to predict peculiar features of the observed gamma-ray flux, such as its anti-correlation with the solar cycle phases. Hence it is crucial to find a theoretical model that explains the mechanisms behind gamma-ray emission. The gamma-ray emission in this energy range is caused by the interaction of galactic cosmic rays with the solar atmosphere. Here we investigate the trajectories of sunward and anti-sunward moving GeV-TeV galactic cosmic rays (protons) as they move within the magnetic field near the solar surface. We performed numerical simulations through the PLUTO code for astrophysical fluid dynamics in which test-particle protons evolve on a static magnetic-arcade field model. Some protons are trapped as they gyrate around the magnetic arcades, some fall toward the Sun's surface, and others escape the magnetic arcade region away from the Sun. We focus on the latter, as these particles escaping from the Sun can produce gamma rays that are observed at Earth.

38th International Cosmic Ray Conference (ICRC2023)
26 July - 3 August, 2023
Nagoya, Japan

ICRC2023
38th International Cosmic Ray Conference
The Astroparticle Physics Conference

*Speaker

© Copyright owned by the author(s) under the terms of the Creative Commons Attribution-NonCommercial-NoDerivatives 4.0 International License (CC BY-NC-ND 4.0).

PoS(ICRC2023)662

1. Introduction

The Sun is the closest bright quiescent source of gamma-rays. It shines both from its disk due to pion decay of multi-GeV or TeV galactic cosmic rays (GCRs) hadrons (mainly protons) interacting with solar atmosphere protons, and from its halo due to inverse Compton (IC) scattering of GCRs electrons and positrons at the same energies on the solar optical photon field. Seckel, Stanev, and Gaisser in 1991 proposed the first (and only to date) theoretical model that explains disk emission, often called the SSG model [1], based on mirroring of the trajectory of GCR protons deeper in the solar atmosphere within magnetic flux tubes.

Soon after its launch in 2008, the observations of the NASA Fermi Gamma-Ray Space Telescope in the gamma-rays band (from 20 MeV to 300 GeV) started questioning the SSG model. Indeed, the flux predicted by SSG was found to be 7 times smaller than the one observed by Fermi-LAT during the minimum of solar cycle 24 (from August 2008 until late 2019) at energies above 100 MeV [2]. Subsequent analysis of solar disk gamma-rays by Fermi between 2008 and 2020 (including two solar minima) uncovered even more surprising and unexpected features. A statistically significant dip in the 30 – 50 GeV energy range persisting both during and after the solar minimum was found [3]. This unexplained spectral dip is not detected by the CALorimetric Electron Telescope (CALET, observing from 1 GeV up to 10 TeV) data collected from November 2015 to September 2020 for a total of 1796 days. However, the size of the statistical errors cannot rule out its presence [4]. Another strange behavior is the large anticorrelation of the flux with solar activity up to $\sim$ 30 GeV observed in Pass 8 by [5]. Moreover, the SSG model has an abrupt cutoff at $E \simeq 5$ GeV while the gamma-ray flux from the disk greatly exceeds their predictions and extends up to $>$ 100 GeV energy. Indeed, [6] observed a gamma-ray flux up to 2.6 TeV with the data collected by the High Altitude Water Cherenkov Gamma-ray Observatory (HAWC), which observes gamma-rays at higher energies (i.e., from 100 GeV to 10 TeV). Finally, it is noteworthy that the observed spectrum is harder than the CR spectrum [7].

The main goal of this work is to develop a new theoretical model for the gamma-ray emission from the solar disk. Test-particle protons simulations are used to investigate the transport of GeV-TeV GCR protons through a kinematic model of a magnetic arcade active region. Our model field also includes a magnetic turbulent component.

2. Theoretical model

2.1 Magnetic arcade model with turbulent component

The magnetic field model shown in Figure 1 consists of a potential-field arcade contained in the xy-plane defined by the vector potential

$$A_z(x, y) = B_0 \Lambda_B \cos\left(\frac{x}{\Lambda_B}\right) e^{-y/\Lambda_B}, \tag{1}$$

where $B_0 = 10/e^{-0.05/\Lambda_B}$ is the magnetic field strength, while $\Lambda_B = L/\pi$ represents the magnetic scale height related to the length of the domain L [8] [see also [9] for a 3D geometry]. The total magnetic field is defined as $\mathbf{B}_{\rm tot}(x, y, z) = \mathbf{B}(x, y) + \delta\mathbf{B}(x, y, z)$, where $\mathbf{B}(x, y)$ represents the static magnetic field defined by the arcades while $\delta\mathbf{B}(x, y, z)$ is the static turbulent component calculated

PoS(ICRC2023)662

by using the prescription in [10]. Remote observations cannot currently constrain the amplitude and geometry of the magnetic fluctuations in the solar atmosphere [see, e.g., 11]. We adopt here the ansatz that $(\delta\mathbf{B}(x,y,z)/\mathbf{B}(x,y))^2 = \sigma^2$ is uniform and that $\delta\mathbf{B}(x,y,z)$ has a three-dimensional isotropic power spectrum $P(k) = [1.0 + (kL_c)^{\delta}]^{-1}$ where $\delta = 11/3$. GCRs can be trapped inside these magnetic arcades and interact to produce gamma-rays. In this work, we plan to assess the effect of the closed magnetic field geometry on the GCR-atmosphere proton collisions on the observed gamma-ray flux.

2.2 GCRs motion and interaction

GCRs motion on the total magnetic field is described by the equations

$$\frac{d\mathbf{x}_p}{dt} = \mathbf{v}_p, \qquad \frac{d(\gamma\mathbf{v})_p}{dt} = \left(\frac{e}{mc}\right)_p \mathbf{v}_p \times \mathbf{B}, \tag{2}$$

where $\mathbf{v}_p$ and $\mathbf{x}_p$ represent the velocity and spatial coordinate respectively, $\gamma = (1 - \mathbf{v}_p^2/c^2)^{-1/2}$ is the Lorentz factor, c represent the speed of light, and $(e/mc)_p$ is the proton charge to mass ratio. The suffix p is indeed used to label protons. As stated in the previous section, solar gamma rays can derive from a GCR proton interacting with another proton from the solar atmosphere, and the interaction time scale for this collision is given by $t_{\rm int}(y) = 1/[n(y)\sigma_c v]$, where $n(y) = n_0 e^{-y/\Lambda_B}$ is the number density, $v = c$ is the typical particles speed, and σ_c is the proton-proton inelastic collisions cross-section, whose parameterization is given by Equation 1 in [12].

3. Initial conditions and particles evolution on the background magnetic field

The PLUTO code for astrophysical gas dynamics is used to carry out the numerical simulations [13]. The initial configuration considers a 2D computational domain of size $L \times L$, where $L = 0.3R_\odot$ ($R_\odot = R_{\rm sun} = 6.957 \times 10^{10}$ cm). In particular, the computational box is defined by $-0.15 < x/R_\odot < 0.15$ and $0 < y/R_\odot < 0.3$. The bottom of the computational domain corresponds to the top of the Sun's photosphere. Consequently, the considered portion of the solar atmosphere, i.e., the bottom of the chromosphere, is in good approximation completely ionized. The mass density at the bottom of the domain is then $\rho_0 \sim 10^{-9}$ g/cm^3 [14], corresponding to a proton number density $n_0 = 10^{15}$ protons/cm^3. The grid resolution is 1000×1000 and we count the number of cells along the y-direction with the j index. The boundary conditions are set to outflow in all directions.

It is important to stress that GCRs are likely to approach the solar atmosphere first by following along open field lines and some of them might migrate to the closed field lines (see right panel of Figure 1). We initially inject 9000 test particle protons positioned one per cell at different altitudes along the y-direction, corresponding to $500 < j < 510$, $600 < j < 610$, $700 < j < 710$, $800 < j < 810$. Particles injected at a $j < 500$ would result from those injected higher up in altitude which reach the lower part of the domain. Protons are initialized with an isotropic velocity distribution defined by

$$v_x = v_0 \sin\theta\cos\phi, \qquad v_y = v_0 \sin\theta \sin\phi, \qquad v_z = v_0 \cos\theta, \tag{3}$$

where $\theta = \arccos(1 - 2\mathcal{R}_{[0,1]})$ and $\phi = 2\pi\mathcal{R}_{[0,1]}$ (see left panel of Figure 1), with $\mathcal{R}_{[0,1]}$ representing a random number between 0 and 1, and v_0 is the velocity magnitude related to different values of

PoS(ICRC2023)662

initial energy: 100 GeV and 10 TeV. We chose the initial isotropic velocity distribution as it incorporates the effect of the turbulence for particles going upward due to the scattering.

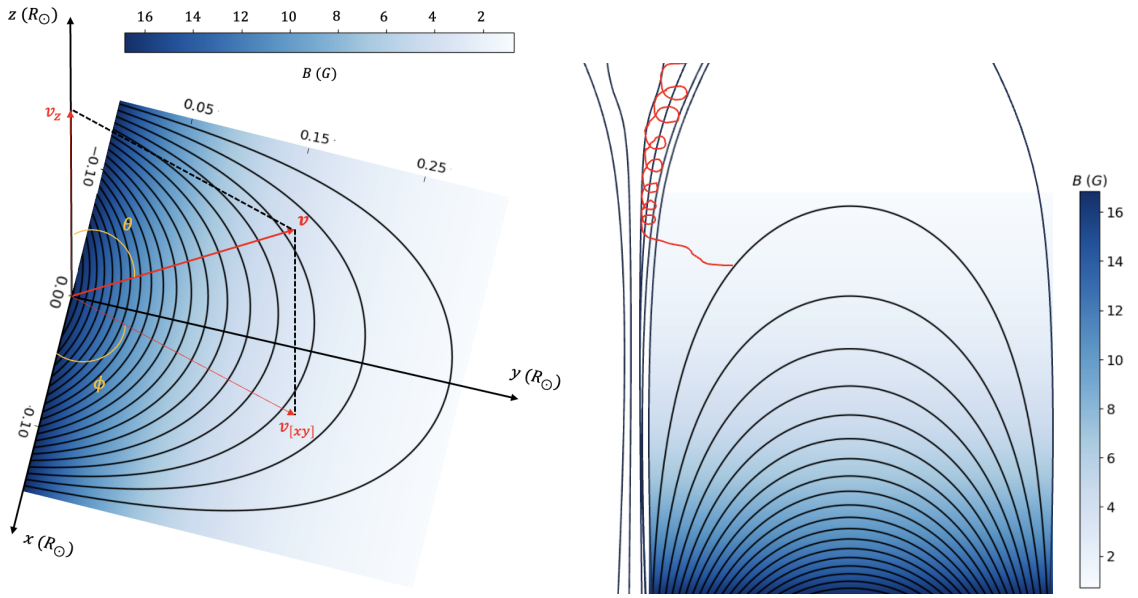

Figure 1: *Left panel*: Schematic decomposition of the particle velocity vector in its components and angular coordinates θ and ϕ over the magnetic arcade domain made of magnetic arcades represented by the solid black curves given by the vector potential A_z (see Equation 1) superimposed on the magnetic field magnitude in blue color scale. *Right panel:* Schematic representation of the trajectory of an approaching GCR (in red) gyrating first along the open field lines and then entering the closed magnetic field lines region.

The turbulence coefficients reported in [10] are calculated at the beginning of the simulation and reshuffled every 100 particles. We choose $L_{\rm min} = 10^{-4} R_\odot$ and $L_{\rm max} = 5 \times 10^4 R_\odot$, the correlation length as $L_c = L/2 = 0.15 R_\odot$, and different values for the wave variance $\sigma^2 = \langle \delta B(x,y,z)^2 \rangle / B(x,y)^2 = 0, 0.01, 0.1, 1$. The particle equations of motion (see Eq. 2) are solved using the Boris algorithm already implemented in the PLUTO code until $t_{\rm stop} = 20 R_\odot / c = 46.4$ s and protons are considered escaped when they leave the computational domain in the $x-y$ plane and/or $z_p < -0.1 R_\odot$ or $z_p > 0.1 R_\odot$ without interacting with ambient protons. We are interested in GCR protons that interact with protons within the solar atmosphere (so with a $t_{\rm int} < \Delta t$, where Δt is the time they spend in the computational box), and with a velocity along the y-direction that is positive ($v_y > 0$), since the gamma-rays produced should be observed at Earth and not absorbed by the Sun.

4. Results

In the absence of turbulence ($\sigma^2 = 0$), particles tend to follow single field lines [10] and may undergo the mirroring process, while they also undergo pitch-angle scattering and cross-field diffusion mechanism when turbulence is present ($\sigma^2 \neq 0$). The diffusion is described by the coefficients $\kappa_\parallel(x,y,v) \propto B^2(x,y)/\sigma^2$ and $\kappa_\perp(x,y,v) \propto \sigma^2/B^2(x,y)$, which are respectively parallel and perpendicular to the average magnetic field. Thus, we investigated the interacting particles position for increasing values of σ^2, injecting them in a horizontal strip within $500 < j <$

PoS(ICRC2023)662

510. Figure 2 captures the position of the outgoing particles at the time of interaction (i.e., $v_y > 0$ and $t_{\rm int} < \Delta t$) color-coded by their z-component for $\sigma^2 = 0$ (left panel) and $\sigma^2 = 1$ (right panel) for the 100 GeV (upper panels) and 10 TeV (lower panels) case. For weak turbulence ($\sigma^2 \ll 1$), particles just follow the magnetic field lines and interact first in the lower part of the domain (where the interaction time is shorter due to the large ambient density), and the mean free path $\lambda_\parallel$, for a given σ^2, is larger (and so is $\kappa_\parallel$) due to the strong magnetic field [see, e.g., 15] and then particles interact at higher altitudes as time increases, with a more efficient mirroring at 100 GeV due to the shorter gyroperiod, compared with the travel time. For strong turbulence ($\sigma^2 = 1$), the position of the particles at the time of interaction is more spread through the domain, since $\kappa_\perp$ increases with σ^2 for both the perpendicular [10] and the cross-field diffusion [16], in particular for the 10 TeV case where the gyroradius is greater than in the 100 GeV case. Indeed, in this case, particles interact at and near the injection position as $\kappa_\perp$ increases with σ^2 while $\kappa_\parallel$ decreases (together with the mean free path $\lambda_\parallel$).

The ratio of the number of particles interacting before leaving the arcade region to the total number of injected particles with a certain range of the y-component for different values of σ^2 and for the two different energies is shown in Figure 3. While the maximum y-component increases with σ^2 in the 10 TeV case (right panel), this does not occur in the 100 GeV case (left panel). Indeed, in this case, particles interact close to the injection position as σ^2 increases, probably due to the smaller gyroradius and mean free path $\lambda_\parallel$.

Figure 4 shows that for the 10 TeV case (right panel) turbulence is essential in trapping particles in magnetic arcades and the larger the turbulence, the more particles interact. Indeed, the solid lines in the right plot show that the number of interacting particles increases with σ^2 at all injection height j, and correspondingly the fraction of escaping particles (dashed lines) smoothly decreases. The same does not occur for the 100 GeV case (left panel), as the gyroradius is smaller, and then particles do not diffuse significantly towards the bottom of the domain (where the interaction time is shorter) but are confined by the strong magnetic field while drifting (and escaping) along the z-direction before interacting. Therefore, we find that the trapping due to turbulence strongly depends on the particles energy. Moreover, the size of the arcade in this model matters. Indeed, a computational domain 5 times smaller with strong turbulence and the same Λ_B? does not efficiently trap even the 100 GeV protons.

5. Conclusions and outlooks

This work leads the way to our search for a theoretical model explaining the gamma-ray emission from the Sun. Turbulence plays a crucial role in trapping GCRs in this preliminary arcade-field model. The efficiency of the trapping mechanism depends on the particles energy: at higher energies (see the 10 TeV case) the number of interacting and escaping particles increases and decreases with σ^2 respectively, while at lower energies (the 100 GeV case) the behavior is not monotonic and is still under investigation. The calculation of the γ-ray flux is underway.

PoS(ICRC2023)662

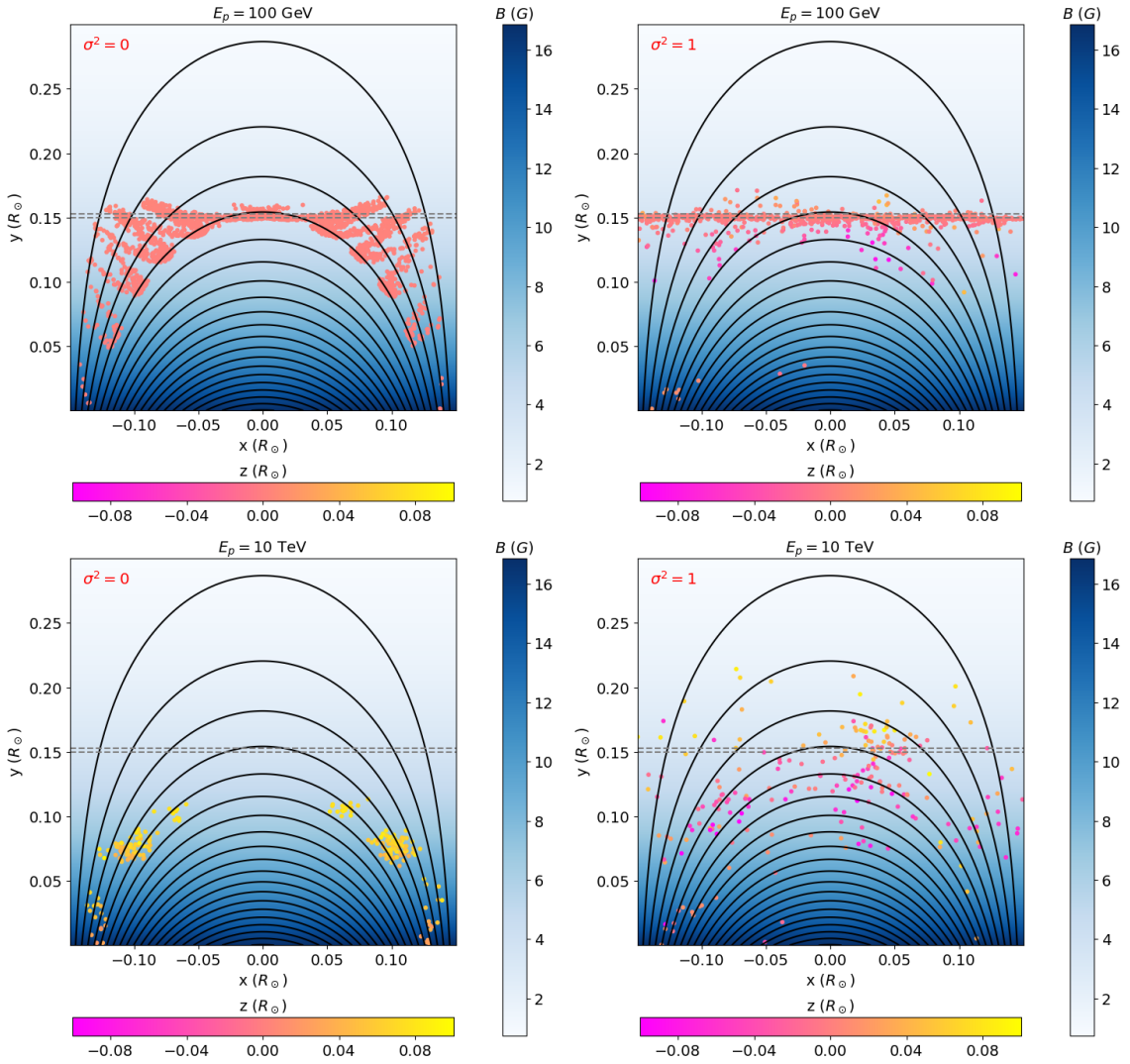

Figure 2: *Left panel*: Magnetic field strength and magnetic arcades with superimposed the position at the interaction time of 100 GeV protons over the whole computational time, color-coded in yellow-pink by their z-component obtained with $\sigma^2 = 0$. The blue color-scale represents the magnetic field magnitude. The dashed gray lines represent the particles injection height. *Right panel:* Same as left panel but with $\sigma^2 = 1$. *Bottom panels:* Same as top panels but fot the 10 TeV case.

Acknowledgements

E.P. was supported by NASA under grant 80NSSC22K0040. F.F. was partially supported by NASA under grants 80NSSC22K0040, 80NSSC18K1213, 80NSSC21K0119 and 80NSSC21K1766. F.F. was also supported, in part, by NASA through Chandra Theory Award No. TM0-21001X, TM6-17001A issued by the Chandra X-ray Observatory Center, which is operated by the Smithsonian Astrophysical Observatory for and on behalf of NASA under contract NAS8-03060. J. K. and J. G. were partially supported by NASA under grant 80NSSC22K0040.

PoS(ICRC2023)662

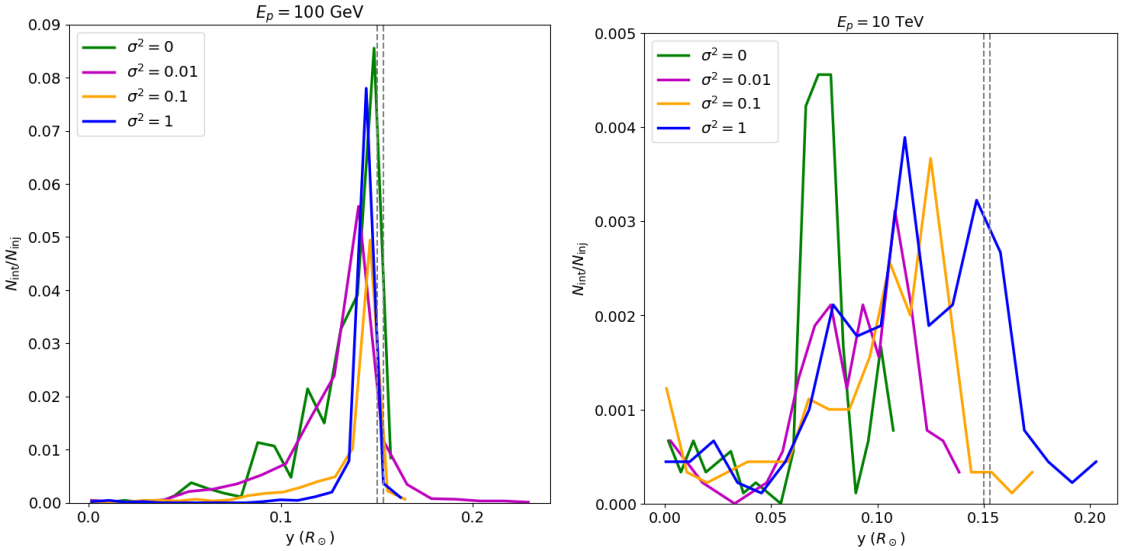

Figure 3: *Left panel*: Ratio of the number of particles interacting before leaving the arcade region to the total number of injected particles as a function of their y-coordinate at the moment of interaction for different values of σ^2 represented by different colors and for the 100 GeV case. The dashed vertical gray lines represent the particles injection height. *Right panel*: Same as left panel but for the 10 TeV case.

References

[1] Seckel D., Stanev T., Gaisser T. K. (1991) *Signatures of Cosmic-Ray Interactions on the Solar Surface*, ApJ, 382, 652.

[2] Abdo A. A., et al. (2011) *Fermi Large Area Telescope Observations of Markarian 421: The Missing Piece of its Spectral Energy Distribution*, ApJ, 736, 131

[3] Tang Q.-W., Ng K. C. Y., Linden T., Zhou B., Beacom J. F., Peter A. H. G. (2018) *Unexpected dip in the solar gamma-ray spectrum*, Phys. Rev. D, 98, 063019

[4] Cannady, N. W. (2022) *Low-energy gamma-ray observations above 1 GeV with CALET on the International Space Station*, 37th International Cosmic Ray Conference, 604

[5] Linden T., Zhou B., Beacom J. F., Peter A. H. G., Ng K. C. Y., Tang Q.-W. (2018) *Evidence for a New Component of High-Energy Solar Gamma-Ray Production*, Phys. Rev. Lett., 121, 131103

[6] Alfaro R., et al. (2023) *The TeV Sun Rises: Discovery of Gamma rays from the Quiescent Sun with HAWC*, Phys. Rev. Lett., 131, 051201

[7] Orlando E., Strong A (2008) *Gamma-ray emission from the solar halo and disk: a study with EGRET data*, A&A, 480, 847

[8] Rial S., Arregui I., Terradas J., Oliver R., Ballester J. L. (2013) *Wave Leakage and Resonant Absorption in a Loop Embedded in a Coronal Arcade*, ApJ, 763, 16

PoS(ICRC2023)662

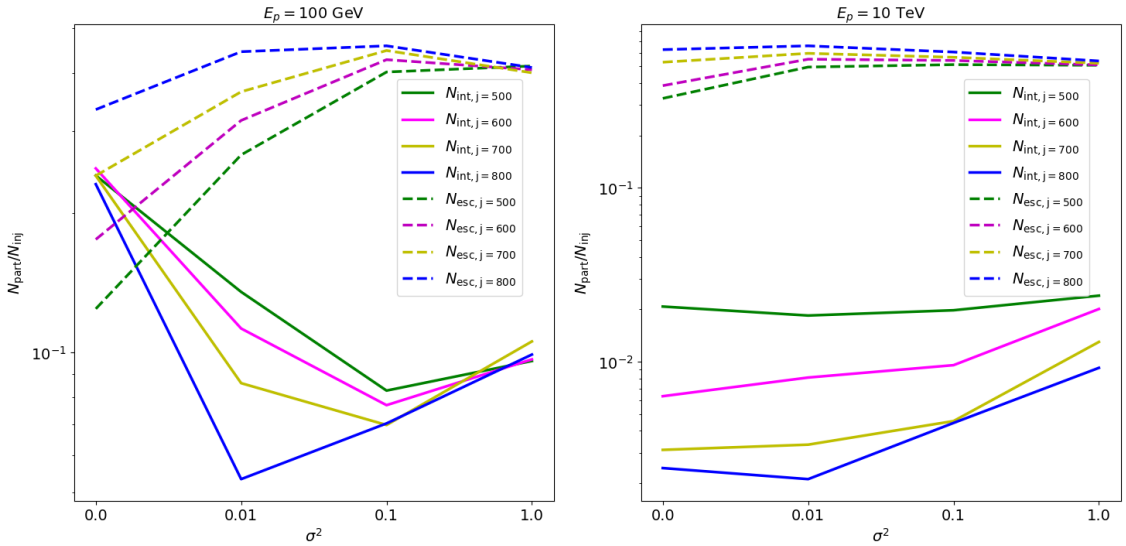

Figure 4: *Left panel*: Number of particles interacting (solid lines) and escaping (dashed lines) divided by the number of injected particles as a function of σ^2 for different values of the injection height, represented by the different colors, for the 100 GeV case. *Right panel*: Same as left panel but for the 10 TeV case.

[9] Zhao X., Xia C., Keppens R., Gan W. (2017) *Formation and Initiation of Erupting Flux Rope and Embedded Filament Driven by Photospheric Converging Motion*, ApJ, 841, 106

[10] Giacalone J., Jokipii J. R. (1999) *The Transport of Cosmic Rays across a Turbulent Magnetic Field*, ApJ, 520, 204

[11] Criscuoli, S., Kazachenko, M., Kitashvili, I., Kosovichev, A., Martínez Pillet, V., Nita, G., Sadykov, V. and Wray, A. (2021) *Challenges and Advances in Modeling of the Solar Atmosphere: A White Paper of Findings and Recommendations*, arXiv:2101.00011

[12] Kafexhiu E., Aharonian F., Taylor A. M. and Vila G. S. (2014) *Parametrization of gamma-ray production cross sections for p p interactions in a broad proton energy range from the kinematic threshold to PeV energies*, Phys. Rev. D, 90, 123014

[13] Mignone A., Bodo G., Massaglia S., Matsakos T., Tesileanu O., Zanni C., Ferrari A. (2007) *PLUTO: A Numerical Code for Computational Astrophysics*, ApJS, 170, 228

[14] MacBride C. D., Jess D. B., Khomenko E., Grant S. D. T. (2022) *Ambipolar Diffusion in the Lower Solar Atmosphere: Magnetohydrodynamic Simulations of a Sunspot*, ApJ, 938, 154

[15] Fraschetti, F., Alvarado-Gómez, J. D., Drake, J. J., Cohen, O. and Garraffo, C. (2022) *Stellar Energetic Particle Transport in the Turbulent and CME-disrupted Stellar Wind of AU Microscopii*, ApJ, 937, 2

[16] Fraschetti F., Jokipii J. R. (2011) *Time-dependent Perpendicular Transport of Fast Charged Particles in a Turbulent Magnetic Field*, ApJ, 734, 83

PoS(ICRC2023)662